High rate failure properties of aortic tissue

M. Rastgar-Agah[1], S. Assari[1], A. Rachev[2] and K. Darvish[1]
[1] Department of Mechanical Engineering, Temple University, Philadelphia, PA
[2] Institute of Mechanics, Sofia, Bulgaria

ABSTRACT

While traumatic aortic rupture (TAR) continues to be a major cause of fatality in motor vehicle accidents, its underlying mechanisms are still not well identified. TAR is believed to be caused by a complex state of loading occurring in only a few milliseconds. A major step to gain insight into the mechanisms of TAR is to understand the high-rate failure properties of aortic tissue. Fresh samples from porcine isthmus region were tested using a new high rate uniaxial extension test setup. Three levels of low, medium, and high strain rates (approximately 3 s^{-1}, 60 s^{-1}, and 300 s^{-1}) were applied in the longitudinal direction and the time histories of stretch ratios and Cauchy stress were determined. The maximum strain rate was increased by 10 folds compared to previous studies. Two states were identified to characterize the tissue failure namely the failure initiation (FI) and the maximum load (ML) states. The FI state was detected from high speed video images and occurred before a noticeable change in force was observed. The ML state was determined directly from force measurements. The trends of stretch ratio and stress in both states were nonlinear. Deterministic models were derived for the FI state parameters. The trends of the ML state parameters were more complex which was attributed to the statistical distribution of collagen fibers undulation. The results suggest that the discrepancies reported in the failure properties of aorta may be due to these more general nonlinear trends.

INTRODUCTION

Traumatic aortic rupture (TAR) is the second leading cause of injury-related fatalities after traumatic brain injury. While TAR has been reported in various incidents such as auto-pedestrian collisions, falls, and crush injuries, car crashes are the most common cause of TAR (Neschis, 2008) with the peri-isthmus region as the most frequent site of rupture (Bertrand 2008). Almost all real-world ruptures of aorta occur in the longitudinal direction with a transverse tear that usually initiates from intima (Stemper et al. 2007, Bertrand 2008).

TAR in car accidents is caused by a complex state of deformation occurring at high rates. The mechanisms of loading that are proposed for TAR include intraluminal pressure increase, longitudinal stretch, direct impact, local osseous pinching, and water hammer effect (Bertrand

1

2008, Neschis 2008). Although mechanical behavior of aorta in physiological condition has been studied before by several research groups, very few studies have investigated the mechanical and failure behavior of aorta in high rate deformations.

Collins and Hu (1972) investigated the rate dependence of cylindrical segments of free-end porcine aorta segments by pressurizing the vessel at two different rates corresponding to nominal logarithmic strain rates of 0.005 s^{-1} and 1-3.5 s^{-1}. They observed an increase in the longitudinal failure stress with nominal values from 300 kPa to 450 kPa with increasing strain rate although no statistical analysis was presented. They also mentioned that failure strain decreases and stiffness increases with an increase in strain rate but no specific values were reported for these measures.

The failure properties of human aortic tissue is reported by Mohan and Melvin (1982). Uniaxial extensions in both circumferential and longitudinal directions at nominal strain rates of 0.01-0.07 s^{-1} and 80-100 s^{-1} were carried out on samples from descending aorta. They reported an increase in longitudinal and circumferential failure stresses from 1.47 and 1.72 MPa to 3.59 and 5.07 MPa. In contrast with what was reported by Collins and Hu (1972), no significant difference in failure stretch ratios were observed. (1.47 and 1.53 in longitudinal and circumferential directions in quasi static loading respectively vs 1.64 and 1.60 in dynamic loading).

In another article, Mohan and Melvin (1983) investigated the failure properties of aortic samples by biaxial bubble inflation experiments at nominal strain rates of 0.01-1 and 20 s^{-1}. They reported a consistent rupture of the sample in longitudinal direction, in conformance with data from real world car crashes, and reported a significant increase in failure stress from average values of 1.14 MPa in quasi-static to 1.96 MPa in dynamic loading. The corresponding stretch ratios were 1.44 and 1.28 which showed a decreasing trend but it was not statistically significant. These results confirmed their uniaxial extension tests results.

The studies mentioned above did not develop any constitutive model for aortic tissue. Bass et al. (2001) characterized a two dimensional Fung type strain energy density function from data obtained by cyclic planar biaxial extension tests on porcine aortic arch samples at two nominal frequencies of 20 and 60 Hz. Their study had the advantage of using the samples from aortic arch which is the most frequent site of TAR; however their model is limited by the number of samples (4 samples), nominal strain rates that have been covered (2 nominal strain rates) and the fact that the strain and stress levels were in the physiological range. They also investigated the rupture properties of aortic tissue by sudden increase in intraluminal pressure of whole human aortas *in situ* and *ex vivo*. They observed no preferred rupture direction for aorta which is in contrast to what has been reported by Mohan and Melvin (1983) and autopsy observations after car accidents (Bertrand 2008). The reported average failure circumferential stretch ratios at distal and proximal aorta were 1.16 and 1.19 while the longitudinal stretch ratio was 1.13. Failure stress values (0.794 and 0.828 MPa for circumferential and 0.397 and 0.414 MPa for longitudinal direction respectively at distal and proximal aorta) are consistent with the numbers reported by Collins and Hu (1972).

Shah et al. (2006) used planar biaxial experiment to test failure properties of cadaveric samples from ascending aorta, peri-isthmus region and descending aorta at two nominal extension rates of 1 m/s and 5 m/s. The strain rates resulted in the tissue show a wide overlap between the

two groups (Lagrangian strain rates of 23-206 s⁻¹ for slow speed and 52-230 s⁻¹ for high speed) and although the average strain rates found to be significantly different (77.86±43.27 s⁻¹ vs 135.90 ±55.34 s⁻¹) no significant difference in mechanical measures were detected. All tissue failures occurred in longitudinal directions similar to real world TAR. Pooling the data from all samples and both extension rates; the average longitudinal and circumferential moduli were found to be 8.87 and 10.57 MPa and failure longitudinal stress and strain were 1.96 MPa and 0.254. Longitudinal stretch tests on whole aorta samples were also carried out at average strain rate of 11.8 s⁻¹ and resulted in average failure engineering stress and Lagrangian strain of 0.75 MPa and 0.221.

In a recent study on failure properties of aorta, Stemper and colleagues (2007) used uniaxial extension test to quantify rate dependence and failure properties of aortic tissue in longitudinal direction. The samples were tested at 4 nominal strain rates of 0.06, 0.6, 6 and 30 s⁻¹. Statistical analysis showed a significantly lower failure strain at the highest strain rate compared to the 1st and 2nd strain rates groups. Similar difference was observed for modulus of elasticity. On the other hand, failure stress in general was observed to increase significantly by strain rate. These results confirm the results of Collins and Hu (1972). Specific values of these failure mechanics were not presented and no constitutive model was characterized based on these data.

As it was explained above, there are discrepancies in the rate dependence of mechanical behavior and ultimate stress/strain of aortic tissue in the literature. The goal of this study was to characterize the rate dependent failure properties of porcine aortic tissue for TAR applications in a wide range of strain rates.

MATERIALS AND METHODS

Five Fresh porcine aortas were obtained from a local slaughterhouse and transported in ice-cold Phosphate Buffered Saline (PBS) to the lab. Porcine aorta is used as a surrogate for young and healthy human aorta. Adipose and connective tissues were removed from the aortas and dumbbell shaped samples (with approximately 10 mm length in 5 mm width gage length) were cut out, using a custom-made punch, at the isthmus region in longitudinal and circumferential directions (Figure 1). This study was focused on 10 longitudinal samples as aorta rupture usually happens in this direction. Samples were kept in 4°C PBS until 30 minutes before the test. The experiments were conducted in room temperature. The thickness of the samples was measured by a customized dial gauge indicator. An array of dots was marked on the intimal side of the samples using a sharpie pen for video tracking.
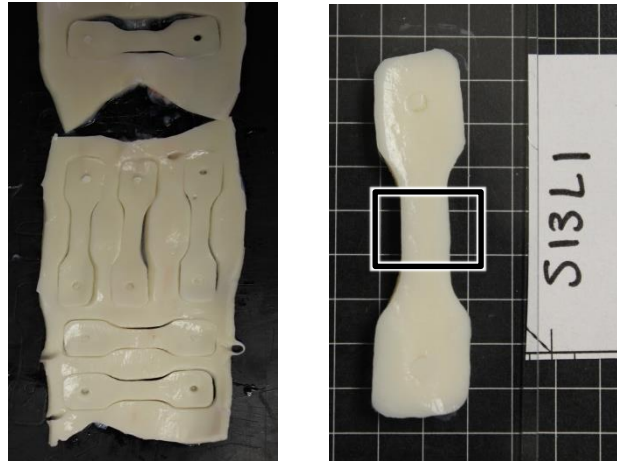
Figure 1- Left) Samples were cut out at the isthmus region of aortas. Right) Samples gage area is shown. The grids are 5 mm.

One goal of this study was to cover the strain rates that are reported in the literature and extend it to 300 s^{-1}. For this purpose, a high rate uniaxial test setup, capable of applying high strain rates on small aorta samples, was designed and built (Figure 2). This setup consists of two support fixtures secured next to a linear impact system (Darvish, 2009) and a moving dynamic crosshead. Aorta sample is held between the load cell support fixture and the dynamic crosshead. The dynamic crosshead consists of a plate with a grip to hold one end of the aorta sample and two PTFE bearings that allow free linear movement along two shafts that are secured on the shafts support fixture. The dynamic cross head is hit by the impact system moving mass and its movement results in uniaxial deformation in the sample. The two support fixtures were separated to reduce the impact vibration noise in the load cell.
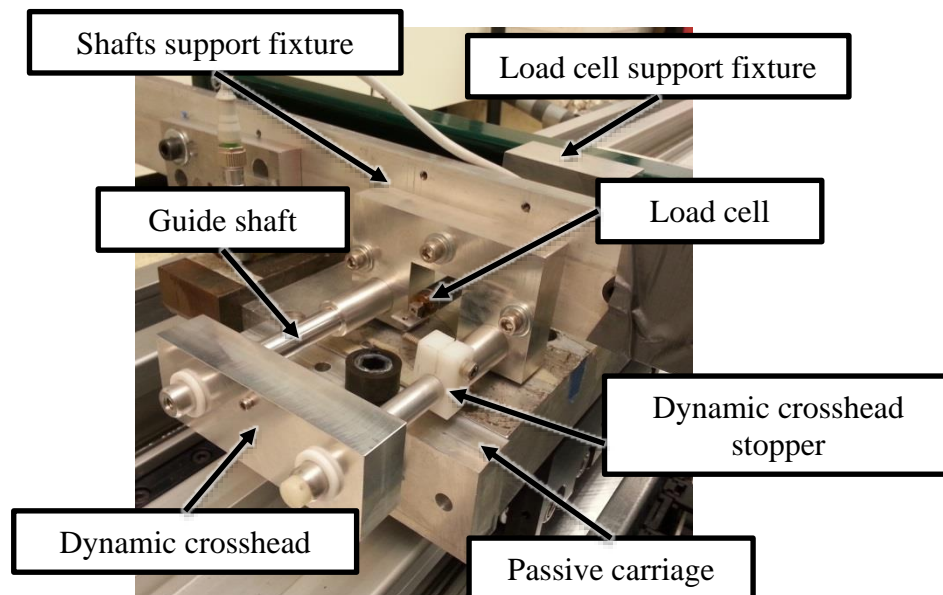

Figure 2-High rate uniaxial test setup.

4

Samples were preconditioned manually with 10 cycles to approximately 20% strain (average physiological strain) and then the initial length of the sample was adjusted by a stopper behind the dynamic crosshead. This initial length corresponded to a small preload (approximately 0.1 N mean value recorded for one second) which was considered to be negligible compared to the failure load. The experiments were carried out with impact speeds of 0.1 m/s (n=3), 1 m/s (n=4) and 5 m/s (n=3) that will be referred to as low, medium, and high rate tests.

A high frequency load cell (25lb, Model 11, Honeywell, Golden Valley, MN) was utilized for force measurement. The deformation of the sample was recorded by a high-speed camera (Phantom v4.2, Vision Research, Wayne, NJ) at 1kHz for low rate and 10 kHz for medium and high rate tests. An inertia compensation accelerometer (Endevco, Meggitt Sensing Systems, Irvine, CA) was mounted to the load cell support fixture. Digital sampling rate of the signals was at 2kHz for low rate and 20 kHz for medium and high rate tests.

For data analysis, the deformation of the sample was assumed to be in a horizontal plane with axes x_1 and x_2 (subscripts 1 and 2) corresponding to directions along and perpendicular to the direction of extension respectively. The first Piola-Kirchoff (1st PK) engineering stress in the extension direction was calculated by

$$P_{11} = \frac{F}{wt} \tag{1}$$

in which F is the recorded force, t is the initial thickness and w is the initial width of the sample. At each time step, the corresponding Cauchy stress was calculated by

$$T_{11} = \lambda_1 P_{11} \tag{2}$$

where λ_1 is the stretch ratio in the extension direction and was measured from videos analysis.

A deformation analysis code was written in MATLAB to calculate the 2D stretch ratios. The position of each marker was tracked in the $x_1 - x_2$ plane and the displacement of each marker was calculated with reference to the first frame. A set of 12 triangular mesh was constructed with the markers at their nodes with 1x3 resolution. The displacement field in each element was assumed to be a linear function of the initial position as

$$\begin{bmatrix} u_1 \\ u_2 \end{bmatrix} = \begin{bmatrix} a_{10} & a_{11} & a_{12} \\ a_{20} & a_{21} & a_{22} \end{bmatrix} \begin{bmatrix} 1 \\ X_1 \\ X_2 \end{bmatrix} \tag{3}$$

where vector $\boldsymbol{u}$ is the displacement field and vector $\boldsymbol{X}$ is constructed from the positions of the markers in the initial frame. Constants a_{ij} were calculated by solving Equation 3 from known vectors $\boldsymbol{u}$ and $\boldsymbol{X}$ at each time step for each element. Assuming no shearing occurred through the thickness of sample and the incompressibility condition, the deformation gradient $\boldsymbol{F}$ was calculated as

$$\boldsymbol{F} = \boldsymbol{I} + \nabla \boldsymbol{u} = \begin{bmatrix} \lambda_1 & a_{12} & 0 \\ a_{21} & \lambda_2 & 0 \\ 0 & 0 & 1/(\lambda_1 \lambda_2) \end{bmatrix} \tag{4}$$

in which $\lambda_1 = 1 + a_{11}$ and $\lambda_2 = a_{22} + 1$ are the stretch ratios. Smallness of a_{12} and a_{21}, compared to the diagonal terms, was used as verification of pure uniaxial deformation.

Figure 3 shows representative result of the deformation analysis code at different stretch ratios. At each time, the variability of λ_1 and λ_2 in elements was negligible and the average values

5

of all elements were considered as stretch ratios of the sample. The initiation of tear or partial failure was detected in the video files. This state was referred to as the failure initiation (FI) state. The stretch ratio and Cauchy stress at the maximum load were referred to as the maximum load (ML) state.
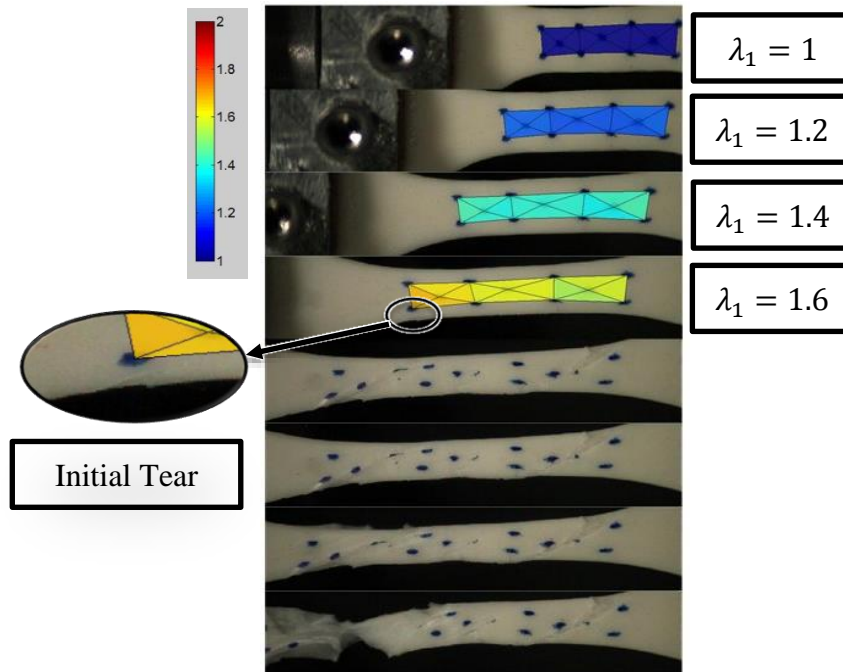

Figure 3 - Sequence of images from initial length to rupture for a representative sample. Color bar shows the stretch ratio in the direction of extension (λ_1). The initiation of tear indicated.

From the collected data, the following parameters are reported in this study:
1- Average Strain rate: the slope of the λ_1 vs t curve before the FI state.
2- FI state parameters: Cauchy stress (T_{11}) and λ_1 corresponding to the time of initiation of tear or partial failure
3- ML state parameters: Cauchy stress (T_{11}) and λ_1 corresponding to the time of peak force or stress.

RESULTS

Figure 4 shows a representative 1st PK stress vs time curves for longitudinal and circumferential samples tested at the medium rate. Partial failure resulted in a significant change in the curvature that was followed by a rise in stress. After the maximum stress was reached, total rupture occurred. The FI state in the longitudinal direction occurred before a noticeable change in the force data. A higher peak stress was observed in the circumferential direction, compared to the longitudinal direction, which is a manifest of anisotropy of the tissue.
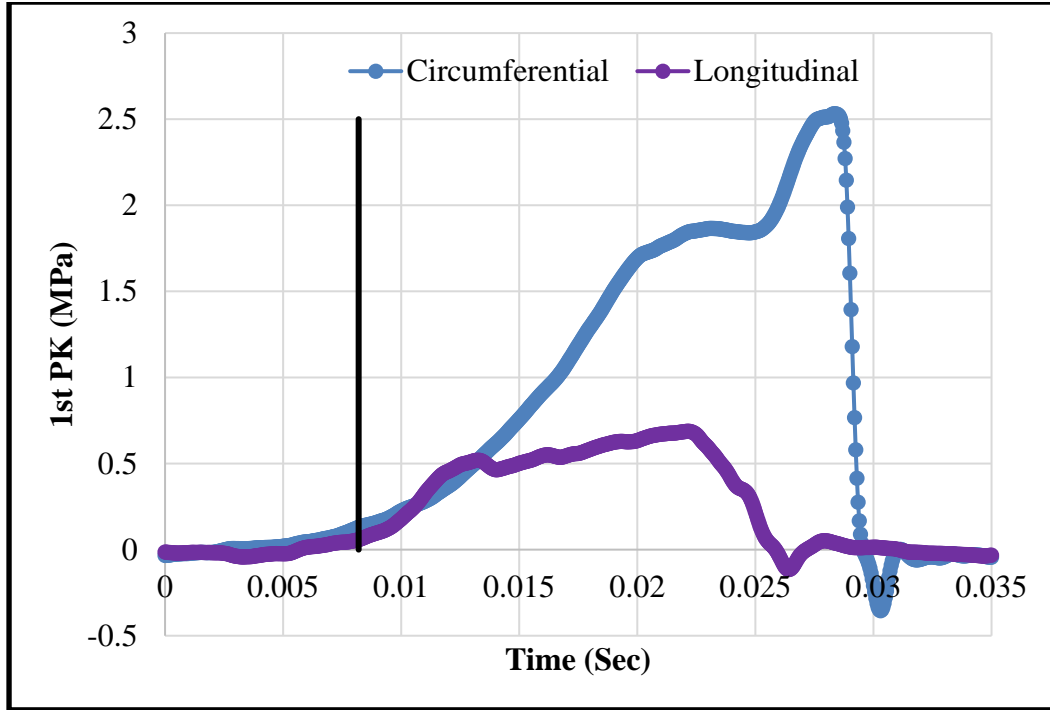
6

Figure 4 – Representative 1st PK stress vs time for circumferential and longitudinal samples tested at medium rate. Each curve consists of elastic region, partial failure, maximum load, and total rupture. Vertical line shows the time of initial failure obtained from videos.

The average (± standard error) of engineering strain rates were found to be 3.1 ± 0.1 s^{-1}, 56.3 ± 1.1 s^{-1}, and 327.2 ± 20.1 s^{-1} for extension in low, medium, and high rate tests respectively. These rates covered the data reported in the literature and increased the maximum strain rate for porcine aorta by 10 folds (Stemper, 2007).

The FI and ML parameters for different strain rates are shown in Figure and 6. Although all trends were nonlinear, the trends related to the FI state showed a smooth increase when plotted against the log of strain rate and showed less variability compared to the ML state trends. For the FI state, the following curve fits were obtained to describe the stretch ratio and Cauchy stress as functions of the strain rate $\dot{\varepsilon}$:

$$\lambda_1 = 1.37 \log(\dot{\varepsilon}) + 0.08, \qquad R^2 = 0.998 \qquad (5)$$
$$T_{11} = 0.74 \log(\dot{\varepsilon})^2 + 0.10 \text{ (MPa)}, \qquad R^2 = 0.987 \qquad (6)$$

The trends observed for the ML state were not deterministic and require more data points at different strain rates. One-way ANOVA showed that the observed differences were not significant for both FI state ($F(2,7) = 4.25, p = 0.06$ for stretch ratio and $F(2,7) = 1.94, p = 0.21$ for stress) and ML state ($F(2,7) = 2.94, p = 0.12$ for stretch ratio and $F(2,7) = 2.17, p = 0.18$ for stress). Since the number of samples was relatively small, the probability of type II error exists ($\beta = 0.46$ and 0.72 for stretch ratio and stress for the maximum load state) and therefore the number of samples should be increased in the future.
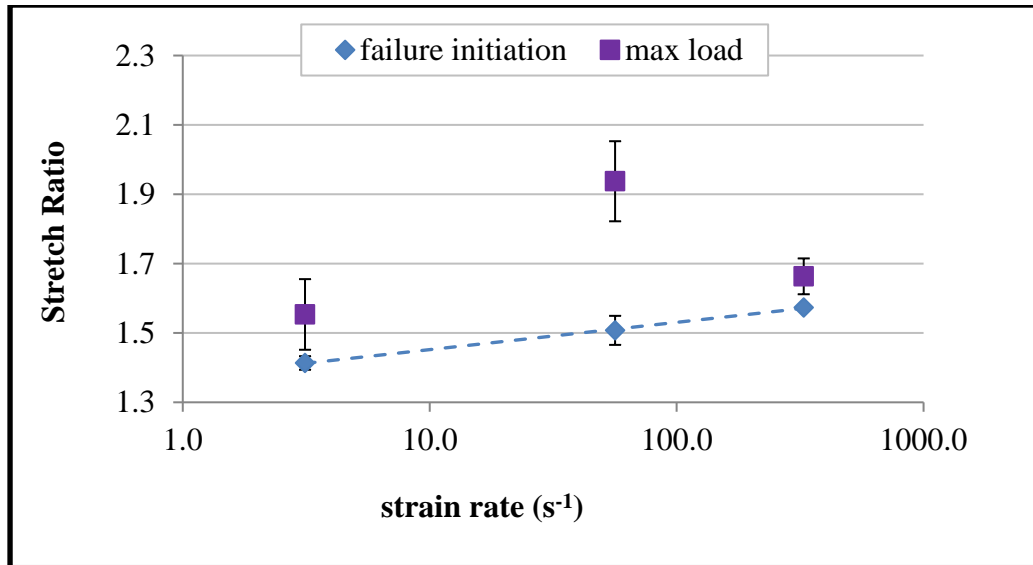
7

Figure 5 – Stretch ratio versus strain rate for FI and ML states. FI fit is a 1st order log curve fit for the FI state. The error bars show the standard error.
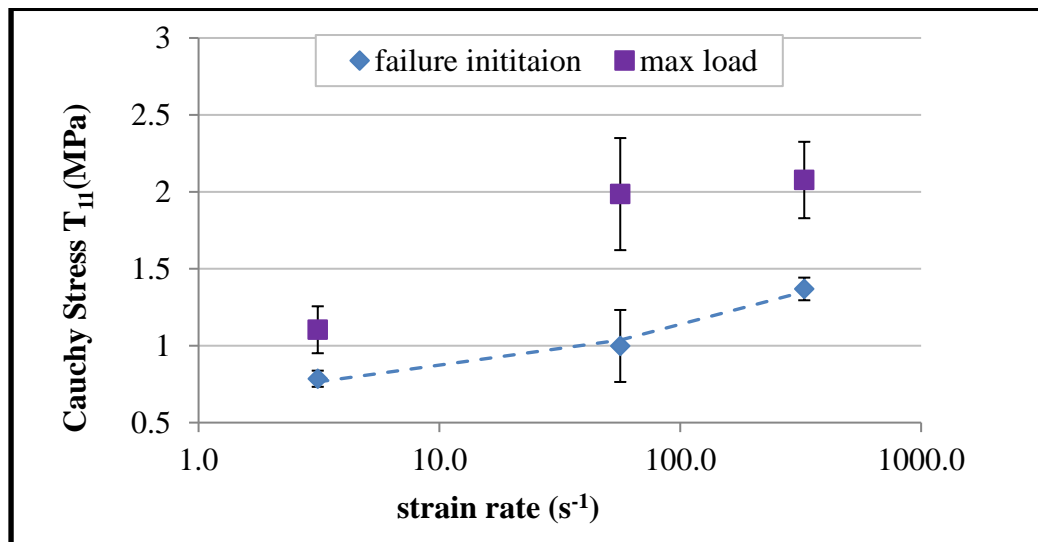

Figure 6 - Cauchy stress versus strain rate for the FI and ML states. FI fit is a 2nd order log curve fit for the FI state. The error bars show the standard error.

DISCUSSION

Although the use of restraint systems has increased in recent years, the overall incidence of blunt aortic injury in car accidents has remained the same (Neschis 2008). Richens and colleagues (2003) by investigating 7,076 car accidents from 1992 to 1999 concluded that airbag and seatbelts did not eliminate the risk of TAR. This emphasizes the necessity of more comprehensive studies on the underlying mechanisms of aortic injuries in order to improve the effectiveness of automobile passenger safety measures. The goal of this work was to study the

8

failure behavior of aortic tissue and characterize its mechanical behavior after initiation of partial failure

The new uniaxial test setup was used to cover a wide range of strain rates and increase the maximum strain rate 10 folds compared to the previous results for porcine aorta (Stemper, 2007). Despite some drawbacks of uniaxial extension experiment for biological tissues, e.g. alteration of physiological geometry (Humphrey, 2002) and the assumption of uniform stress through the thickness of tissue (Labrosse, 2012), it was chosen for this study since applying the high strain rates beyond 300 s^{-1} is currently not feasible in other test modes including inflation/extension tests and planar biaxial tests.

Two states related to aorta failure were distinguished in this study. In addition to the ML state, which is commonly considered in previous studies, the FI state was also considered. The FI state is important in mechanical modeling of the tissue since after this state a viscoelastic hyperelastic model will no longer work and a model of partial failure needs to be considered. Aortic tissue in the isthmus region is an elastic artery and primarily consists of elastic lamellae (made of concentric layers of elastin) and collagen fibers that run primarily in the circumferential direction (Holzapfel, 2006). Based on the results of this study, the failure mechanism of aorta can be partly explained. Collagen fibers are naturally undulated and become more stretched as the load is increased and this results in a toe region followed by a linear region in the elastic part of the stress-strain curve. Failure initiation occurs when stretched fibers start to fail mechanically and as a result other fibers become stretched. Consequently the apparent elastic modulus varies slightly and is then increased before the maximum load is reached. It is expected that the ML state parameters would be less deterministic than the FI state parameters since the statistical distribution of the fiber undulation adds to the sample to sample variability.

The trends of the ML state parameters were compared with two comparable studies reported in the literature. Stemper *et al.* (2007) and Mohan and Melvin (1982) showed increase of maximum stress with strain rate which was in agreement with the results of this study. In terms of the failure stretch ratio, Stemper and colleagues (2007) observed that it decreases with strain rate while Mohan and Melvin (1982) reported no changes. Our results showed a nonlinear trend for failure stretch ratio versus strain rate that peaked at the medium rate. This finding indicates that depending on which range of strain rate being considered, different local trends can be observed. Clearly more data is needed to explain the discrepancies reported in the literature with statistical significance.

Aortic tissue is anisotropic as it was shown in the significant difference between longitudinal and circumferential maximum stresses in Figure 4. The degree of this anisotropy and the orientation of any preferred directions are debatable. The results of this study showed that the a_{12} term in Equation (4) was less than 5% of the diagonal terms. This means that, with 5% error, directions 1 and 2 used in this study can be considered as the principal axes of an orthotropic material. This finding is consistent with the result of other researchers, e.g. Sacks (2000) and Holzapfel and Ogden (2009).

One of the limitations of this work is that we were looking at the intimal side of the tissue to detect the initiation of failure. Stemper et al. (2007) used two high speed cameras and recorded

the experiment from both sides of the sample. They reported that the initiation of failure always occurred at intima which supports our choice of placing the camera on the intimal side. However, since aortic tissue has multiple layers, any partial failure that started from within the layers (for example slippage of the layers with respect to each other) cannot be detected with our method.

CONCLUSIONS

This work is a preliminary study on the high rate failure properties of aortic tissue. A new high rate uniaxial test setup was utilized that was capable of inducing strain rates from 3 s^{-1} to 300 s^{-1} in small samples of porcine aorta. Variation of Cauchy stress and stretch ratio in the longitudinal direction with respect to strain rate were studied and two states of failure initiation and maximum load were distinguished. The results showed that the discrepancies reported in the failure properties of aorta may be due to more general nonlinear trends of failure parameters with respect to strain rate. The presented results provide a step forward in our understanding of partial and total failure of aorta that is needed to characterize the failure mechanisms that lead to TAR.

ACKNOWLEDGEMENTS

REFERENCES

Bass, C. R., Darvish, K., Bush, B., Crandall, J. R., Srinivasan, S. C., Tribble, C., ... & Wang, C. (2001). Material properties for modeling traumatic aortic rupture. Stapp car crash journal, 45, 143.

Bertrand, S., Cuny, S., Petit, P., Trosseille, X., Page, Y., Guillemot, H., & Drazetic, P. (2008). Traumatic rupture of thoracic aorta in real-world motor vehicle crashes. Traffic injury prevention, 9(2), 153-161.

Collins, R., & Hu, W. C. L. (1972). Dynamic deformation experiments on aortic tissue. Journal of biomechanics, 5(4), 333-337.

Darvish, K., Shafieian, M., Romanov, V., Rotella, V., Salvatore Jr., M. D. , and Blebea, J. (2009). Development of an In vitro Porcine Aorta Model to Study the Stability of Stent Grafts in Motor Vehicle Accidents. Journal of Biomechanical Engineering, 131 (4), 044505:1-4.

Holzapfel, G. A. (2006). Determination of material models for arterial walls from uniaxial extension tests and histological structure. Journal of theoretical biology, 238(2), 290-302.

Holzapfel, G. A., & Ogden, R. W. (2009). On planar biaxial tests for anisotropic nonlinearly elastic solids. A continuum mechanical framework. Mathematics and mechanics of solids, 14(5), 474-489.

10

Humphrey, J. D., & Na, S. (2002). Elastodynamics and arterial wall stress. Annals of biomedical engineering, 30(4), 509-523.

Labrosse, M. R., Gerson, E. R., Veinot, J. P., & Beller, C. J. (2013). Mechanical characterization of human aortas from pressurization testing and a paradigm shift for circumferential residual stress. Journal of the mechanical behavior of biomedical materials, 17, 44-55.

Lee, M. C., & Haut, R. C. (1992). Strain rate effects on tensile failure properties of the common carotid artery and jugular veins of ferrets. Journal of biomechanics, 25(8), 925-927.

Mohan, D., & Melvin, J. W. (1982). Failure properties of passive human aortic tissue. I—uniaxial tension tests. Journal of biomechanics, 15(11), 887-902.

Mohan, D., & Melvin, J. W. (1983). Failure properties of passive human aortic tissue. II—biaxial tension tests. Journal of Biomechanics, 16(1), 31-44.

Monson, K. L., Goldsmith, W., Barbaro, N. M., & Manley, G. T. (2003). Axial mechanical properties of fresh human cerebral blood vessels. Journal of biomechanical engineering, 125(2), 288-294.

Neschis, D. G., Scalea, T. M., Flinn, W. R., & Griffith, B. P. (2008). Blunt aortic injury. New England Journal of Medicine, 359(16), 1708-1716.

Richens, D., Kotidis, K., Neale, M., Oakley, C., & Fails, A. (2003). Rupture of the aorta following road traffic accidents in the United Kingdom 1992–1999. The results of the co-operative crash injury study. European journal of cardio-thoracic surgery, 23(2), 143-148.

Sacks, M. S. (2000). Biaxial mechanical evaluation of planar biological materials. Journal of elasticity and the physical science of solids, 61(1-3), 199-246.

Schulman, C. I., Carvajal, D., Lopez, P. P., Soffer, D., Habib, F., & Augenstein, J. (2007). Incidence and crash mechanisms of aortic injury during the past decade. The Journal of Trauma and Acute Care Surgery, 62(3), 664-667.

Shah, C. S., Hardy, W. N., Mason, M. J., Yang, K. H., Van Ee, C. A., Morgan, R., & Digges, K. (2006). Dynamic biaxial tissue properties of the human cadaver aorta. Stapp car crash journal, 50, 217-246.

Stemper, B. D., Yoganandan, N., & Pintar, F. A. (2007). Mechanics of arterial subfailure with increasing loading rate. Journal of biomechanics, 40(8), 1806-1812.